TOWARDS PREDICTABLE FEATURE ATTRIBUTION: REVISITING AND IMPROVING GUIDED BACKPROPAGATION

Anonymous authors
Paper under double-blind review

ABSTRACT

Recently, backpropagation(BP)-based feature attribution methods have been widely adopted to interpret the internal mechanisms of convolutional neural networks (CNNs), and expected to be human-understandable (lucidity) and faithful to decision-making processes (fidelity). In this paper, we introduce a novel property for feature attribution: predictability, which means users can forecast behaviors of the interpretation methods. With the evidence that many attribution methods have unexpected and harmful phenomena like class-insensitivity, the predictability is critical to avoid over-trust and misuse from users. Observing that many intuitive improvements for lucidity and fidelity tend to sacrifice predictability, we propose a new visual explanation method called TR-GBP (Theoretical Refinements of Guided BackPropagation) which revisits and improves GBP from theoretical perspective rather than solely optimizing the attribution performance. Qualitative and quantitative experiments show that TR-GBP is more visually sharpened, gets rid of the fidelity problems in GBP, and effectively predicts the possible behaviors so that we can easily discriminate some prediction errors from interpretation errors. The codes of TR-GBP are available in supplementary and will be open source.

1 INTRODUCTION

Feature attribution methods seek to assign importance or relevance scores for each of input features, thus users can understand the decision-making processes of deep models. The original BP-based attribution calculates saliency(Simonyan et al., 2013), the absolute values of raw gradients. As saliency usually provides results which are mixed with noise and hard to understand, many attribution methods have been proposed to improve the visualization *lucidity*. While the lucidity of BP-based attributions developed rapidly, some studies reveal that many widely deployed attribution methods do not meet expectations of humans and suffer from the following problems: different classes might obtain similar attributions (Tsunakawa et al., 2019), attribution results could keep the same even if the models are randomized (Adebayo et al., 2018), or explanations may not reflect the true changes of the input images (Subramanya et al., 2019), and etc. These results raise concerns about the *fidelity* of feature attribution methods, and some theoretical studies have attempted to explain these phenomena (Nie et al., 2018; Sixt et al., 2020). Different from previous studies, we focus on another question: beyond lucidity and fidelity, is it possible that we can also foresee the possible problems in advance rather than explain them afterwards?

For BP-based attribution methods, predictability do not get enough attention. Actually, there is a gray rhino that has been overlooked by researchers: existing BP-based methods severely lack theoretical *predictability*. Specifically, predictability means that *users are able to predict the possible behaviors of a given cause* (Chakraborti et al., 2019). It is obvious that this property is essential for users to understand the functionalities and limitations of attribution methods. For example, if we cannot predict the possible attribution results for the correct models, we are not able to determine whether an abnormal dependency shown in interpretations indicates an prediction error or just an interpretation error. Therefore, even if an attribution method satisfies lucidity and fidelity, without predictability, users can still hardly make sure that the method works in order or not, which possibly leads to over-trust or misuse phenomena as shown in (Kaur et al., 2020).

Since predictability is so crucial, why are existing methods not able to achieve it? In fact, saliency has a degree of predictability since it represents the local behaviors of models, and if we slightly perturb the input, the output will perform as shown in saliency. However, such predictability disappears when many strategies are used to improve its lucidity, like modifying the backpropagation rules, aggregating the results of different inputs, combining middle activations and backpropagations, and etc. These methods increase lucidity while changing the functionality in an ambiguous way, so we cannot predict the attribution behaviors as before.

Is there a method enjoying lucidity and predictability? Guided BackPropagation (GBP) (Springenberg et al., 2014) might be a good answer as it visualizes well and has a reconstruction theory (Nie et al., 2018) justifying its behaviors. However, GBP has two fidelity problems: the class-insensitivity (Mahendran & Vedaldi, 2016) and the independency of the model parameters (Adebayo et al., 2018). If we also use heuristic strategies as before, we may run the risk of compromising predictability. Therefore, we propose a new approach that no longer optimizes attribution performance directly, but addresses the issues of the reconstruction theory, so-called TR-GBP(Theoretical Refinements of Guided BackPropagation). As a consequence, TR-GBP can solve fidelity problems without losing lucidity or predictability. Our main contributions can be summarized three-fold:

- In addition to lucidity and fidelity, we introduce a novel and critical property *predictability* for BP-based feature attributions.
- We propose a new predictable feature attribution method TR-GBP, by addressing two fundamental issues in the reconstruction theory of GBP.
- Qualitative and quantitative experiments are performed and show that TR-GBP can obtain sharper visualizations, get rid of the fidelity problems of GBP, and enables us to discriminate some prediction errors from interpretation errors.

2 Predictability of Feature Attribution

To get a predictable interpretation, the definition and requirements of predictability should be clarified. In this section, we specify the scope of predictability and provide some specific predictability tasks. Then, we show why heuristic strategies fail to predict behaviors and obtain some tips for keeping predictability when improving the attribution methods.

2.1 Definition of Predictability

Scopes As a reference, in another area, predictability refers to the degree that correct forecasting can be made (Xu et al., 2019). But for BP-based attributions, the forecasting tasks are not naturally determined, so we need to specify the scope of the tasks. Considering that the ultimate goal of model explanations is helping people understand and trust the target models, we focus on the attribution results that can be clearly perceived by humans and the status of the components which decide the decision processes. Specifically, the interpretation results that humans can perceive need to be easily described like intensity changes, shapes, noise, edges, completeness of regions, and etc, while the components that associate with decision processes of a model normally involve model inputs, weights, activations, connections of neurons, and etc. Therefore, predictability can be defined intuitively as the capabilities to predict the human-understandable interpretation behaviors of a given decision-making process.

Measurements After clarifying the definition, how to measure the predictability of an attribution method? Due to the difficulties of constructing a general evaluation framework, we only choose a class of queries which satisfy the human-understandable and are related to the target decision-making process, like how much noise may appear in the interpretation results? What might happen when we let some of the model weights be randomly initialized? If there is an unrelated dependency in the explanation results, does it originate from the model prediction errors or from the explanation itself? How are attribution results actually connected to decision-making? These questions are not trivial for BP-based methods, so predictability can be shown as the capabilities of answering these questions with theoretical analysis.

2.2 REQUIREMENTS OF PREDICTABILITY

As the scopes and tasks of predictability have been clarified, we will next look at what kind of attributions can keep predictability. Recently, there are roughly three kinds of improvement strategies of BP-based attributions: modifying the backpropagation rules, aggregating the results of different inputs, and combining middle activations with backpropagations.

Modifying BP-rules These methods modify the backpropagation rules to obtain noise-less attribution results, like Deconv(Zeiler & Fergus, 2014), Guided Back Propagation(GBP) (Springenberg et al., 2014), Layer-wise relevance propagatoin(LRP) (Bach et al., 2015), ExcitationBP (Zhang et al., 2018), DeepLIFT (Shrikumar et al., 2017), DeepTaylor(Montavon et al., 2017), PatternAttribution (Kindermans et al., 2017), Bias Backpropagation(BBp) (Wang et al., 2019), FullGrad (Srinivas & Fleuret, 2019). However, these changes of backpropagation rules will certainly alter the attribution behaviors, so these methods no longer represent the local behaviors in a small neighbor of a given input, and we cannot specify the functionalities of them until another theory is proposed to justify the behaviors, just like GBP.

Aggregating Gradients Some methods attempt to alleviate gradient issues with the help of the other input gradients, like SmoothGrad (Smilkov et al., 2017) VarGrad(Adebayo et al., 2018) IntegratedGradients (IG) (Sundararajan et al., 2017) BlurIG(Xu et al., 2020) Guided IntegratedGradients (GIG) (Kapishnikov et al., 2021). Note that these methods are all unstable as the choices of other inputs are not determined and different choices might result in different attributions. Therefore, predictability is ruined by uncertainty.

Activation-based Attributions Activation-based explanations provide attributions for a single input with a linear weighted combination of activation maps from convolutional layers, like Class Activation Mapping(CAM) (Zhou et al., 2016), GradCAM (Selvaraju et al., 2017), GradCAM++ (Chattopadhay et al., 2018), NormGrad (Rebuffi et al., 2020), CAMERAS (Jalwana et al., 2021). Remindering that the target convolutional networks are highly non-linear and usually seen as blackboxes, the middle-layer activation maps of CNNs are also blackboxes. Then, the use of activation maps will make these methods have unpredictable components.

In all, these improvement strategies can enhance lucidity, but all fail at predictability. So if we want to optimize an attribution approach, we should find a new way that can insure rigorous functionality, attribution stability, and without unpredictable components.

3 BACKGROUND

As our proposed method is based on the reconstruction theory (Nie et al., 2018), we introduce its main conclusions and the core steps of proofs before further discussions.

3.1 PRELIMINARY

Let us start by defining some notations. Consider a multi-category classification with K-class, suppose there is a d-dimensional image $\mathbf{x} = \{x_1, ..., x_d\} \in \mathbb{R}^d$, its label is $y \in \{1, ..., K\}$, for convenience, we study nomalized input $||\mathbf{x}|| = 1$. We put $\mathbf{x}$ into a deep neural network function $f : \mathbb{R}^d \mapsto \mathbb{R}^K$, then the attribution map for k^{th} class is $R_k : \mathbb{R}^d \mapsto \mathbb{R}^d$. Specifically, W^l is the weight of l^{th} layer of f, $\mathbf{A}^l$ is a vector of the activations of l^{th} layer, and DNN f has L layer. We have the forward propagation:

$$\mathbf{A}^l = \sigma(W^{l\ T}\mathbf{A}^{l-1}) \tag{1}$$

where $\mathbf{A}^0 = \mathbf{x}$. The ReLU function is a widely used activation function $\sigma(x) = (x, 0)_+$:

$$f = W^{L\ T}\mathbf{A}^{L-1} = W^{L\ T}(\prod_{l=1}^{L-1} M^{(L-l)}W^{(L-l)\ T})\mathbf{x} \tag{2}$$

where $M^l = diag(\mathbb{I}(W^{l\ T}\mathbf{A}^{l-1}))$ denotes the gradient mask of the ReLU operation, $\mathbb{I}(\cdot)$ output 1 if input greater than 0, else output 0. Then the original gradient attribution is:

$$R_k = \frac{\partial f_k}{\partial \mathbf{x}} = (\prod_{l=1}^{L-1} W^l M^l)\mathbf{v}_k \tag{3}$$

where $\mathbf{v}_k$ is k^{th} row of $W^{L\ T}$ which can produce the k^{th} output. For GBP, the negative gradients passing through the activation functions will be zero-out with the help of ReLU operation, see Figs.1(b):

$$R_k = \frac{\partial^g f_k}{\partial^g \mathbf{x}} = (\prod_{l=1}^{L-1}(W^l)M^l\sigma\circ)\mathbf{v}_k \tag{4}$$

3.2 Reconstruction Theory of GBP

There are two main results of reconstruction theory (Nie et al., 2018): one is a theorem for three-layer CNNs and the other is a proposition for expanding to deeper networks. Now we consider a three-layer CNN, consisting of an input layer, a convolutional hidden layer and a fully connected layer. Let $W \in \mathbb{R}^{p\times N}$ be N convolutional filters and we denote each column $w^{(i)}$ as the i-th filter with size p. Then, we let $C \in \mathbb{R}^{p\times J}$ be J image patches extracted from $\mathbf{x}$, and each column $c^{(j)}$ with size p is generated by a linear function $c^{(j)} = D_j\mathbf{x}$ where $D_j \triangleq [0_{p\times(j-1)s}\ \ I_{p\times p}\ \ 0_{p\times(d-(j-1)s-p)}]$ with s being the stride size. The weights in the fully connected layer can be represented by $V \in \mathbb{R}^{NJ\times K}$. Therefore, the k-th logit is represented by

$$f_k(\mathbf{x}) = \sum_{i=1}^{N}\sum_{j=1}^{J} V_{q_{ij},k}\sigma(w^{(i)T}c^{(j)}) \tag{5}$$

where the index q_{ij} denotes the $((i-1)J+j)$-th entry in every column vector of weight matrix V .

Theorem 1. *Considering a three layer ReLU convolutional network with sufficient large like Eqn.(5), and the elements of V and W are all assumed to be independently Gaussian distributed with zero mean and variance c^2, Z is the normalized term, and GBP at the k-th logit is:*

$$s_k^{GBP}(\boldsymbol{x}) = \frac{\partial^g f_k}{\partial^g \boldsymbol{x}} = \frac{1}{Z}\sum_{j=1}^{J} D_j^T \sum_{i=1}^{N} w^{(i)}\mathbb{I}(w^{(i)}c^{(j)})\sigma(V_{q_{ij},k}) \tag{6}$$

Then, the GBP at the k-th logit can be approximated as:

$$s_k^{GBP}(\boldsymbol{x}) \approx \frac{2c^2pN}{\pi C_0 Z}\boldsymbol{x} \tag{7}$$

where $C_0 = ||c^{(j)}||_2$ and if we assume they are the same for all j, then use the normalization term $Z = \frac{\pi C_0}{2c^2pN}$, we have $s_k^{GBP}(\boldsymbol{x}) \approx \boldsymbol{x}$.

Nie et al. (2018) provide a proof of Theorem 1, and now we briefly demonstrate the key proof steps: (1) They transform the summations into the mean of filter weights: $\sum_{i=1}^{N} w^{(i)}\mathbb{I}(w^{(i)}c^{(j)})\sigma(V_{q_{ij},k}) = N\frac{1}{N}\sum_{i=1}^{N} w^{(i)}\mathbb{I}(w^{(i)}c^{(j)})\sigma(V_{q_{ij},k})$. (2) They estimate this mean with the help of the expectation of weight distributions: $\frac{1}{N}\sum_{i=1}^{N} w^{(i)}\mathbb{I}(w^{(i)}c^{(j)})\sigma(V_{q_{ij},k}) \approx \mathbb{E}(w^{(i)}\mathbb{I}(w^{(i)}c^{(j)})\sigma(V_{q_{ij},k}))$. (3) Note that all the weights sampled i.i.d, the expectations can be split into a product of two items: $\mathbb{E}(w^{(i)}\mathbb{I}(w^{(i)}c^{(j)}))$ and $\mathbb{E}(\sigma(V_{q_{ij},k}))$. (4) $\mathbb{E}(\sigma(V_{q_{ij},k}))$ are constant positive values and $\mathbb{E}(w^{(i)}\mathbb{I}(w^{(i)}c^{(j)})) = \frac{2c^2p}{\pi||c^{(j)}||_2 Z}c^{(j)}$ due to the ReLU operations block the convolutional kernels in the opposite directions to the input $c^{(j)}$, as illustrated in Figs.2(a), the blue arrow represents the input vector where the red arrows mean the weights of convolutional kernels, and a plane perpendicular to input vector blocks out the red arrows which have a large angle with the input. Note that the weights are i.i.d. drawn from Gaussian distributions, the expectations of the rest weights will converge in the same direction as input. (5) If we assume $C_0 = ||c^{(j)}||_2$, each piece $c^{(j)}$ are then arranged according to conventional operations (see Figs.2(b)) and finally normalized to the input $\mathbf{x}$. This result can also be expanded to more than three layers:

Proposition 1. *For a random deep CNN where weights are i.i.d. Gaussians with zero mean, we can also approximate every entry of $\tilde{V}$ as i.i.d. Gaussian with zero mean, where $\tilde{V} = \frac{\partial^g f_k}{\partial^g \boldsymbol{A}^1}$ denotes the backpropation results to the first activation maps.*

The core of this proof is the Gaussian distribution with zero mean, which can use the Central Limit Theorem to obtain. It can be seen that under this theory the functionalities and behaviors of GBP have a theoretical justification for predictions, but a reconstruction might not be a good attribution: the reconstruction represents the use of input information. Note that the predictions of different classes might share similar information, such reconstructions fail to highlight the differences which determine the decision making. In addition, previous work finds that GBP stays identical even if the top layers are randomized (Adebayo et al., 2018). These fidelity issues illustrate the functional deficiencies of the GBP.

4 THEORETICAL REFINEMENT OF GBP

4.1 ADDRESSING THE LIMITATIONS OF RECONSTRUCTION THEORY

Next, we are going to complement some improvements of GBP to obtain fidelity without losing predictability. According to the requirements listed in Section 2.2, keeping predictability needs a theory justifying the behaviors, and the improvements should not apply instable or unpredictable components. Therefore, we decide to obtain ideas for improvements by addressing theoretical shortcomings, so that our changes can also be estimated with this theory. Specifically, we find two limitations:

- **The missing of bias terms**: As reconstruction theory does not take the widely adopted bias terms into consideration, its conclusions cannot be directly applied to traditional networks. As bias terms also contribute to decision-making processes (Srinivas & Fleuret, 2019; Wang et al., 2019), the missing of bias terms will make attribution results incomplete and ignore the high-layer changes. That is why GBP failed the sanity checks (Adebayo et al., 2018).
- **The similarity of $\tilde{V}$**: according to the central limited theorem and the Proposition 1, the backpropagation results might have similar distributions for different $\mathbf{v}_k$, and so that GBP is class-insensitive (Sixt et al., 2020).

These limitations are obvious and gravely affect the fidelity of GBP. Now, we will provide two straight forward strategies without any instable or unpredictable component like other inputs or middle-layer activations. Our improvements are as follows:

(a) *Treatment of bias terms*: We apply an operation commonly used in machine learning to transform the bias term into additional input $\mathbf{1}$: $f(\mathbf{x}) = V\sigma(W\mathbf{x}+b) = V\sigma(\hat{W}\hat{\mathbf{x}})$, where $\hat{W} = [W, b]$, $\hat{\mathbf{x}} = [\mathbf{x}, \mathbf{1}]^T$. As for convolutional networks, the additional input $\mathbf{1}$ will also transform to patches, as illustrated in Figs.1(b):

$$f_k(\mathbf{x}) = \sum_{i=1}^{N}\sum_{j=1}^{J} V_{q_{ij},k}\sigma(w^{(i)T}D_j\mathbf{x}+b) = \sum_{i=1}^{N}\sum_{j=1}^{J} V_{q_{ij},k}\sigma(w^{(i)T}D_j\mathbf{x}+\frac{\mathbf{b}^T}{||D_j||}D_j\mathbf{1}) \tag{8}$$

where $\mathbf{b}$ is a p-dimensional vector filled with b. Therefore, the reconstruction of input $\mathbf{x}$ in Theorem 1 can be divided into two parts: the recovery of input image $\mathbf{x}$, denoted as $\tilde{R}_k^0 = \frac{\partial^g f^k}{\partial^g \mathbf{x}}$, and the recovery of l^{th} layer input $\mathbf{1}^l$, denoted as $\tilde{R}_k^l = \frac{\partial^g f_k}{\partial^g \mathbf{1}^l}$. Then, if we apply the GBP to a model, we need not only obtain the GBP for input image $\mathbf{x}$, but also the middle layer input $\mathbf{1}$, as shown in Figs.1(a). Considering that the model captures different levels of input features, the reconstruction of middle layer $\mathbf{1}$ can reflect the reconstruction abilities at different levels. Note that the final attribution maps must keep the same size of the input $\mathbf{x}$, we aggregate these results with the spatial pior introduced by GradCAM (Selvaraju et al., 2017):

$$\tilde{R}_k = \tilde{R}_k^0 + \sum_l \psi(\tilde{R}_k^l) = \frac{\partial^g f_k}{\partial^g \mathbf{x}} + \sum_l \psi(\frac{\partial^g f_k}{\partial^g \mathbf{1}^l}) \tag{9}$$

where $\psi(\cdot) = BilinearUpsample(\cdot)$.

(b) *Removing similarities shared by different classes*: The goal of attribution is to explain why the model makes a certain decision, so we should focus on what is different across classes, rather than the similar information:

$$R_k(x) = \tilde{R}_k - \frac{1}{K}\sum_{i=1}^{K}\tilde{R}_i \tag{10}$$

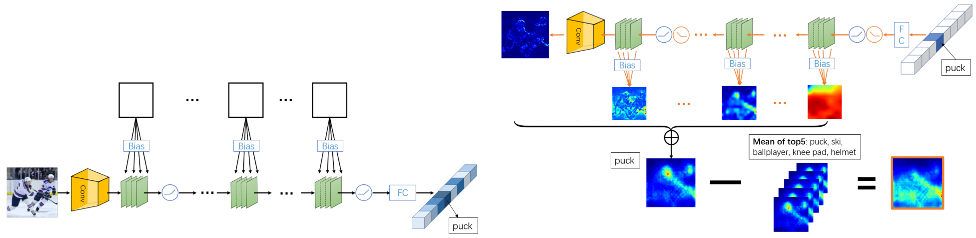

(a) Forward propagation (b) Backward propagation

Figure 1: Pipeline of TR-GBP. The forward propagation treats the bias as input maps fullfilled with 1, and the back propagation procedure also attribute to the middle inputs. Then we aggregate these middle input with upsampling, and minus the mean values of top5 results.

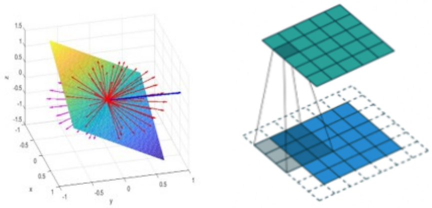

(a) Input alignment (b) Convolution

Figure 2: The illustration of important operations.

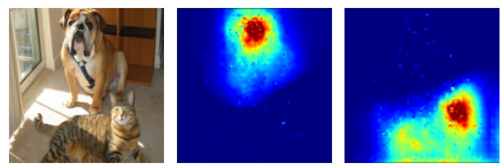

(a) input (b) bull mastiff (c) tiger cat

Figure 3: Class discriminative results for TR-GBP. The middle heatmap is obtained from the class 'bull mastiff', and the right heatmap is obtained from the class 'tiger cat'.

In practice, categories with low prediction probabilities might not have any activated M^L in Eqn.(2), so their backpropagations might be set to zero after the fc-layer, and fail to reflect the shared information. In this work, we therefore remove the mean value of the top5 classes for avoid such absences and achieve computational efficiency. Now, we finally obtain an attribution method R_k, and call it TR-GBP (Theoretical Refinements of Guided BackPropagation). If we want to get different levels of attribution, we can also apply such operation to the middle-layer results: $R^l_k(x) = \tilde{R}^l_k - \frac{1}{K}\sum_{i=1}^{K}\tilde{R}^l_i$. According to the exchangeability of linear operators, we have $R_k = R^0_k + \sum_l \psi(R^l_k)$. The pipeline of TR-GBP is illustrated in Figs.1(b), it can be seen that the puck class uses the information of head and sticks, but if we remove the means of top5 classes: puck, ski, ballplayer, knee pad, helmet, the attribution results become jersey and sticks, as head information is shared with ballplayer or helmet.

4.2 The Predictability of TR-GBP

As predictability has been concretized to some questions in Section 2, we now show how much predictability TR-GBP achieves by answering these questions:

(1) *How much noise may appear in the interpretation results?*

The noise is from the step (2) in Section 3.2, since the estimate of the expectations may introduce differences in randomness. From (Lugosi & Mendelson, 2019), We can set $N = \tilde{O}(p/\epsilon^2)$ such that with high probability $||\frac{1}{N}\sum_{i=1} N\mathbb{I}(w^{(i)}c^{(j)}) - \mathbb{E}(\mathbb{I}(w^{(i)}c^{(j)})|| < \epsilon$, where p denotes the filter size and $\tilde{O}(\cdot)$ hides some other factors. So filter size p and filter num N are the dominant factors for noise. As the top layer normally has larger N, there must be less noise on the top-layer attributions than the bottom-layer results. This phenomenon can be found in Appendix B.

(2) *What might happen to the interpretation results when we let some of the model parameters be randomly initialized?*

According to Theorem 1, if all the weights are randomly initialized, the result will be a recovery of input. As the middle-layer inputs are feature maps fullfilled with 1, the reconstruction will also

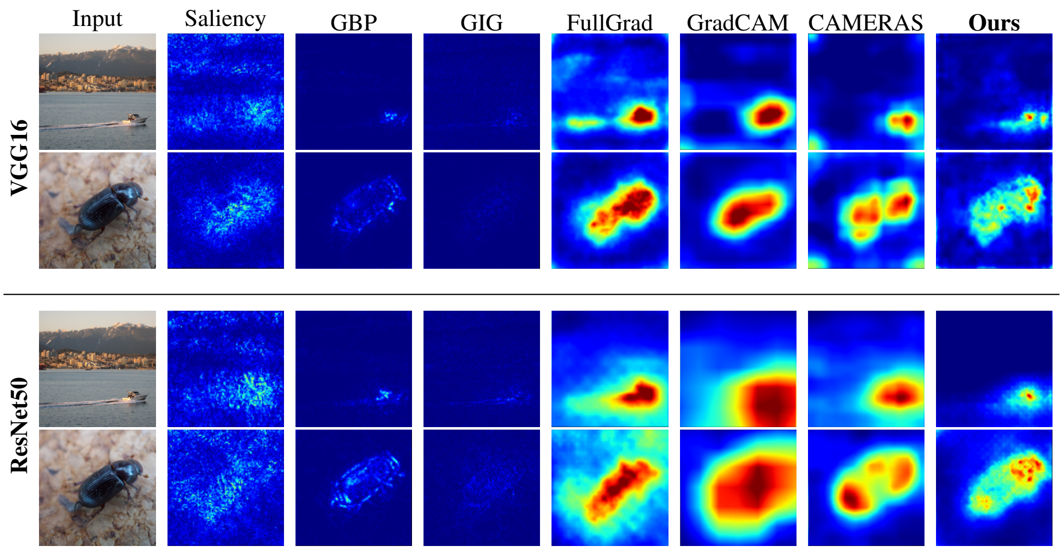

Figure 4: Visualization results on VGG16 and ResNet50 of saliency, GBP, GIG, FullGrad, GradCAM, CAMERAS and our method TR-GBP.

be nearly uniform. Note that boundary inputs usually have less convolutional operators, as shown in Figs.2(b), the center inputs participate 9 convolutions while the corner inputs only have 4 convolutions. So the reconstruction will produce weaker attributions at the boundaries. Therefore, if we cascadely randomize the weights from top layer to the bottom layer, the middle attributions will gradually become uniform. Such phenomenon is shown in Section 5.2.2 and Appendix B.

(3) *When there is an unrelated dependency in the explanation results, does this dependency originate from the prediction errors of the model or from the explanation itself?*

Note that we have predicted that the boundaries of attribution must be weaker, so if there are high scores in boundaries, it must originate from prediction errors. This claim is supported by the results of Section 5.4.

5 Experiments

In this section, we conduct experiments to show that our method can keep lucidity, fidelity, and predictability simultaneously.

5.1 Visual Inspection

We perform qualitative visual evaluation for TR-GBP along with baselines on validation set of ImageNet: saliency, GBP, GIG, GradCAM, FullGrad, CAMERAS. These methods are the newest or the most classical attribution methods of three kinds of attributions listed in Section 2.2. Furthermore, we use the commonly used pretrained models: VGG16 and ResNet50 from torchvision model zoo. The results are shown in Figure 4, it can be seen that saliency is full of noise, GBP and GIG highlight the edges and FullGrad, GradCAM, TR-GBP shed light on a complete region. This is not surprising that TR-GBP is more complete than GBP and more tightly confined to object regions than GradCAM, FullGrad, CAMERAS, because we supplement the bias attributions for GBP and theoretical guarantee low noise level in Section 4.2.

5.2 Fidelity Problems

Note that GBP has found two fidelity problems in previous studies, we need to show that TR-GBP can solve them effectively with our theoretical refinements.

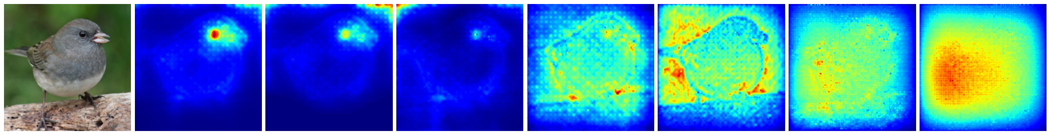

(a) input (b) raw (c) fc (d) layer4 (e) layer3 (f) layer2 (g) layer1 (h) conv1

Figure 5: Sanity check results by cascade randomizing resnet50 from fc layer to the conv1 layer for TR-GBP.

Table 1: Comparative evaluation on Energy-Based Pointing Game (higher is better).

Model(%)	Saliency	GBP	GIG	FullGrad	GradCAM	CAMERAS	Ours
VGG	40.2±0.3	56.1±0.4	41.2±0.6	41.3±0.4	45.7±1.1	45.9±1.0	**52.2±1.4**
ResNet	36.9±0.5	55.4±0.5	40.6±0.7	35.0±0.6	40.8±1.0	50.1±1.2	**53.4±1.1**

5.2.1 Class Discriminative Visualization

Figure 3 shows our results on *cat and dog* image for ResNet50. The top1 class of output is 'bull mastiff' and the top2 class is 'tiger cat'. It is evident that our method can distinguish different classes, and provide entire objects except for the tail of the cat. Such results are reasonable as we remove the reconstruction shared by different categories. More comprehensive results about class discriminative visualizations can be seen in Appendix A.

5.2.2 Sanity Checks

Adebayo et al. (2018) point out that some attribution methods are not able to show the differences between different models, just like special edge detectors. Specifically, they randomize some layers of model, and find that some attribution results, especially GBP, almost remain unchanged. We also perform a sanity check of TR-GBP and present the results in Figure 5. As can be seen, our method is sensitive to model parameters and can efficiently reflect the differences between models before and after randomization. Moreover, the attribution results of TR-GPB converge to uniform with weak boundaries and random noises. This phenomenon just supports the analysis of predictability question (2) in Section 4.2. Other results can be seen in Appendix B.

5.3 Quantitative Evaluations

5.3.1 Localization Abilities

Wang et al. (2020) provide an Energy-Based Pointing Game (EBPG) to evaluate the localization ability of attribution methods. Such evaluation reflects whether the highlighting regions of method are consistent with humans. Specifically, the evaluation is attributed inside the bounding boxes as a proportion of all attributions:

$$EBPG = \frac{\sum R_{x \in bbox}}{\sum R_{x \in bbox} + \sum R_{x \notin bbox}} \tag{11}$$

The experiment settings are shown in Appendix C, and the evaluation results of VGG16 and ResNet50 are reported in Table 1. TR-GBP outperforms all other baseline attribution methods significantly, except GBP. That is because GBP is only part of our attribution and loses a lot of useful information: for example, our method finds many boundary dependencies which associate with prediction errors in Section 5.4, but GBP discards middle-layer information and lacks this capability.

5.3.2 Pixel Perturbations

Pixel perturbations (Samek et al., 2016) are evaluations which remove the most or least important pixels and compare the magnitude of the changes to judge whether the interpretation results effectively describe the models. We perform two kinds of pixel perturbations on Imagenet 2012

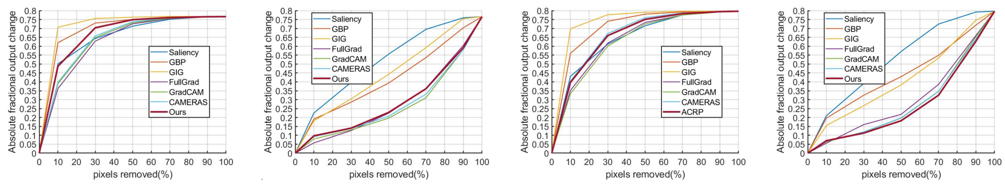

(a) VGG+MoRF (b) VGG+LeRF (c) ResNet+MoRF (d) ResNet+LeRF

Figure 6: Pixel perturbation results on Imagenet 2012 validation set with VGG16 and ResNet50, both removing most relevant features(MoRF,higher is better) and removing least relevant features(LeRF, lower is better).

Table 2: Comparative evaluation on AUC of IBD (higher is better).

Model(%)	**Saliency**	**GBP**	**GIG**	**FullGrad**	**GradCAM**	**CAMERAS**	**Ours**
VGG	52.84	53.03	53.85	53.72	56.86	57.00	**60.95**
ResNet	51.44	51.96	53.79	54.04	53.06	54.99	**62.16**

validation dataset: removing most relevant input features (MoRF) and removing least relevant input features (LeRF) Samek et al. (2016). More details of experiments can be found in Appendix D. The results are shown in Figure 6, as can be seen, our method shows the best result for ResNet+LeRF, outperform CAMERAS, GradCAM, Fullgrad for all MoRF, and obtains comparable performance in VGG+LeRF.

5.4 Validate Predictability

Let us look closely at the results of Figs.5(b) and (c), the changes of fc layer lead to high scores in boundaries. According to the answers to predictability question (3) in Section 4.2, as we have predicted that the boundaries of attribution must be weaker, if there are high scores in boundary pixels of TR-GBP, it must originate from model prediction errors. Note that such boundary dependencies are also shown by previous methods, like CAMERAS in Figs.4. Therefore, we attempt to conduct validation experiments to make sure such boundary dependencies in our method are actually a prediction errors but others not. Specifically, we use a metric which is similar to EBPG to represent the intensities of boundary dependencies (IBD):

$$IBD = \frac{\sum R_{x \in boundary}}{\sum R_{x \in boundary} + \sum R_{x \notin boundary}} \tag{12}$$

where boundary is the 16-pixel boundary regions: $height, width < 16$ or $height, width > 224 - 16$. We dicard half data in ImageNet validation set with the minimal IBD to obtain attribution results with salient boundary dependencies. Note that the dependency originates from prediction errors must have capacities to show the correctness of predictions, so we use traditional AUC (Area Under Curve) values of ROC curve to measure whether IBD can be used as a valid indicator to judge the correctness of model predictions. The results are shown in Table 2. TR-GBP has remarkable advance performance, which means that the boundary dependencies in TR-GBP are actually derived from prediction errors while other methods not, so TR-GBP succeeds in disentangling prediction errors from interpretation errors with the help of predictability.

6 Conclusion

In this work, we propose a novel and important concept *Predictability* for BP-based attributions, and a new attribution method, named TR-GBP, which addresses the issues of reconstruction theory rather than intuitive improvements of performance to improve lucidity and fidelity while ensuring predictability. The experiments on ImageNet show that TR-GBP achieves lucid visualization and solves two fidelity problems. In addition, the answers to predictability questions are all supported by experimental phenomena, so TR-GBP is a predictable attribution method to a certain extent. In the feature, we plan to obtain quantitative evaluations for predictability.

References

Julius Adebayo, Justin Gilmer, Michael Muelly, Ian Goodfellow, Moritz Hardt, and Been Kim. Sanity checks for saliency maps. *arXiv preprint arXiv:1810.03292*, 2018.

Sebastian Bach, Alexander Binder, Grégoire Montavon, Frederick Klauschen, Klaus-Robert Müller, and Wojciech Samek. On pixel-wise explanations for non-linear classifier decisions by layer-wise relevance propagation. *PloS one*, 10(7):e0130140, 2015.

Tathagata Chakraborti, Anagha Kulkarni, Sarath Sreedharan, David E Smith, and Subbarao Kambhampati. Explicability? legibility? predictability? transparency? privacy? security? the emerging landscape of interpretable agent behavior. In *Proceedings of the international conference on automated planning and scheduling*, volume 29, pp. 86–96, 2019.

Aditya Chattopadhay, Anirban Sarkar, Prantik Howlader, and Vineeth N Balasubramanian. Grad-cam++: Generalized gradient-based visual explanations for deep convolutional networks. In *2018 IEEE winter conference on applications of computer vision (WACV)*, pp. 839–847. IEEE, 2018.

Mohammad AAK Jalwana, Naveed Akhtar, Mohammed Bennamoun, and Ajmal Mian. Cameras: Enhanced resolution and sanity preserving class activation mapping for image saliency. In *Proceedings of the IEEE/CVF Conference on Computer Vision and Pattern Recognition*, pp. 16327–16336, 2021.

Andrei Kapishnikov, Subhashini Venugopalan, Besim Avci, Ben Wedin, Michael Terry, and Tolga Bolukbasi. Guided integrated gradients: An adaptive path method for removing noise. In *Proceedings of the IEEE/CVF Conference on Computer Vision and Pattern Recognition*, pp. 5050–5058, 2021.

Harmanpreet Kaur, Harsha Nori, Samuel Jenkins, Rich Caruana, Hanna Wallach, and Jennifer Wortman Vaughan. Interpreting interpretability: Understanding data scientists' use of interpretability tools for machine learning. In *Proceedings of the 2020 CHI Conference on Human Factors in Computing Systems*, pp. 1–14, 2020.

Pieter-Jan Kindermans, Kristof T Schütt, Maximilian Alber, Klaus-Robert Müller, Dumitru Erhan, Been Kim, and Sven Dähne. Learning how to explain neural networks: Patternnet and patternattribution. *arXiv preprint arXiv:1705.05598*, 2017.

Gábor Lugosi and Shahar Mendelson. Sub-gaussian estimators of the mean of a random vector. *The annals of statistics*, 47(2):783–794, 2019.

Aravindh Mahendran and Andrea Vedaldi. Salient deconvolutional networks. In *European Conference on Computer Vision*, pp. 120–135. Springer, 2016.

Grégoire Montavon, Sebastian Lapuschkin, Alexander Binder, Wojciech Samek, and Klaus-Robert Müller. Explaining nonlinear classification decisions with deep taylor decomposition. *Pattern Recognition*, 65:211–222, 2017.

Weili Nie, Yang Zhang, and Ankit Patel. A theoretical explanation for perplexing behaviors of backpropagation-based visualizations. In *International Conference on Machine Learning*, pp. 3809–3818. PMLR, 2018.

Sylvestre-Alvise Rebuffi, Ruth Fong, Xu Ji, and Andrea Vedaldi. There and back again: Revisiting backpropagation saliency methods. In *Proceedings of the IEEE/CVF Conference on Computer Vision and Pattern Recognition*, pp. 8839–8848, 2020.

Wojciech Samek, Alexander Binder, Grégoire Montavon, Sebastian Lapuschkin, and Klaus-Robert Müller. Evaluating the visualization of what a deep neural network has learned. *IEEE transactions on neural networks and learning systems*, 28(11):2660–2673, 2016.

Ramprasaath R Selvaraju, Michael Cogswell, Abhishek Das, Ramakrishna Vedantam, Devi Parikh, and Dhruv Batra. Grad-cam: Visual explanations from deep networks via gradient-based localization. In *Proceedings of the IEEE international conference on computer vision*, pp. 618–626, 2017.

Avanti Shrikumar, Peyton Greenside, and Anshul Kundaje. Learning important features through propagating activation differences. In *International Conference on Machine Learning*, pp. 3145–3153. PMLR, 2017.

Karen Simonyan, Andrea Vedaldi, and Andrew Zisserman. Deep inside convolutional networks: Visualising image classification models and saliency maps. *arXiv preprint arXiv:1312.6034*, 2013.

Leon Sixt, Maximilian Granz, and Tim Landgraf. When explanations lie: Why many modified bp attributions fail. In *International Conference on Machine Learning*, pp. 9046–9057. PMLR, 2020.

Daniel Smilkov, Nikhil Thorat, Been Kim, Fernanda Viégas, and Martin Wattenberg. Smoothgrad: removing noise by adding noise. *arXiv preprint arXiv:1706.03825*, 2017.

Jost Tobias Springenberg, Alexey Dosovitskiy, Thomas Brox, and Martin Riedmiller. Striving for simplicity: The all convolutional net. *arXiv preprint arXiv:1412.6806*, 2014.

Suraj Srinivas and François Fleuret. Full-gradient representation for neural network visualization. *arXiv preprint arXiv:1905.00780*, 2019.

Akshayvarun Subramanya, Vipin Pillai, and Hamed Pirsiavash. Fooling network interpretation in image classification. In *Proceedings of the IEEE/CVF International Conference on Computer Vision*, pp. 2020–2029, 2019.

Mukund Sundararajan, Ankur Taly, and Qiqi Yan. Axiomatic attribution for deep networks. In *International Conference on Machine Learning*, pp. 3319–3328. PMLR, 2017.

Hideomi Tsunakawa, Yoshitaka Kameya, Hanju Lee, Yosuke Shinya, and Naoki Mitsumoto. Contrastive relevance propagation for interpreting predictions by a single-shot object detector. In *2019 International Joint Conference on Neural Networks (IJCNN)*, pp. 1–9. IEEE, 2019.

Haofan Wang, Zifan Wang, Mengnan Du, Fan Yang, Zijian Zhang, Sirui Ding, Piotr Mardziel, and Xia Hu. Score-cam: Score-weighted visual explanations for convolutional neural networks. In *Proceedings of the IEEE/CVF Conference on Computer Vision and Pattern Recognition Workshops*, pp. 24–25, 2020.

Shengjie Wang, Tianyi Zhou, and Jeff Bilmes. Bias also matters: Bias attribution for deep neural network explanation. In *International Conference on Machine Learning*, pp. 6659–6667. PMLR, 2019.

Paiheng Xu, Likang Yin, Zhongtao Yue, and Tao Zhou. On predictability of time series. *Physica A: Statistical Mechanics and its Applications*, 523:345–351, 2019.

Shawn Xu, Subhashini Venugopalan, and Mukund Sundararajan. Attribution in scale and space. In *Proceedings of the IEEE/CVF Conference on Computer Vision and Pattern Recognition*, pp. 9680–9689, 2020.

Matthew D Zeiler and Rob Fergus. Visualizing and understanding convolutional networks. In *European conference on computer vision*, pp. 818–833. Springer, 2014.

Jianming Zhang, Sarah Adel Bargal, Zhe Lin, Jonathan Brandt, Xiaohui Shen, and Stan Sclaroff. Top-down neural attention by excitation backprop. *International Journal of Computer Vision*, 126 (10):1084–1102, 2018.

Bolei Zhou, Aditya Khosla, Agata Lapedriza, Aude Oliva, and Antonio Torralba. Learning deep features for discriminative localization. In *Proceedings of the IEEE conference on computer vision and pattern recognition*, pp. 2921–2929, 2016.

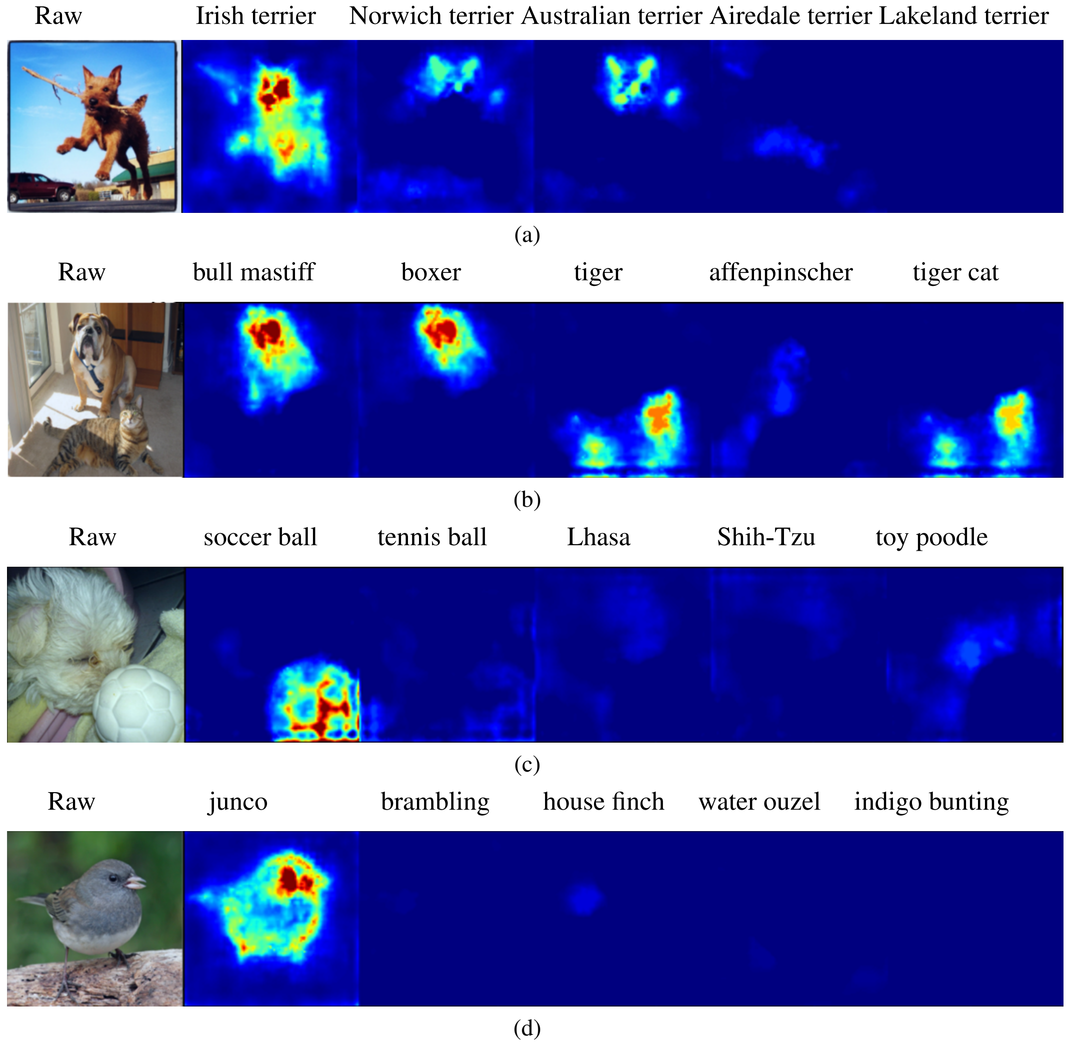

Figure 7: Class Discriminative Visualization for VGG16. From left to right, they represent top1-top5 classes.

A APPENDIX

A CLASS DISCRIMINATIVE VISUALIZATIONS

There are class discriminative visualizations for VGG16 and ResNet50 models. We show the top 5 classes results of TR-GBP in Figure 7 and Figure 8. We use Relu function to highlight the regions which have superior reconstructive abilities than average for the given class. It is shown that TR-GBP can highlight the correct regions for target classes according to their meaning, while absence class would be below the average. For example, in Figure 7(a), the ears of dogs attribute much to Norwich terrier class. In Figure 1(b), all the dog classes highlight the region of dog, and the class of tiger or cat highlights the region of cat. In Figure 7(c), soccer ball and tennis ball show the attention on ball, Lhasa, and etc. show the attention on dog. In Figure 7(d), the junco class is so outstanding that other classes are all below the average. We can also find similar results in Figure 8. These results show that our method can effectively capture the model preferences of input features for different classes.

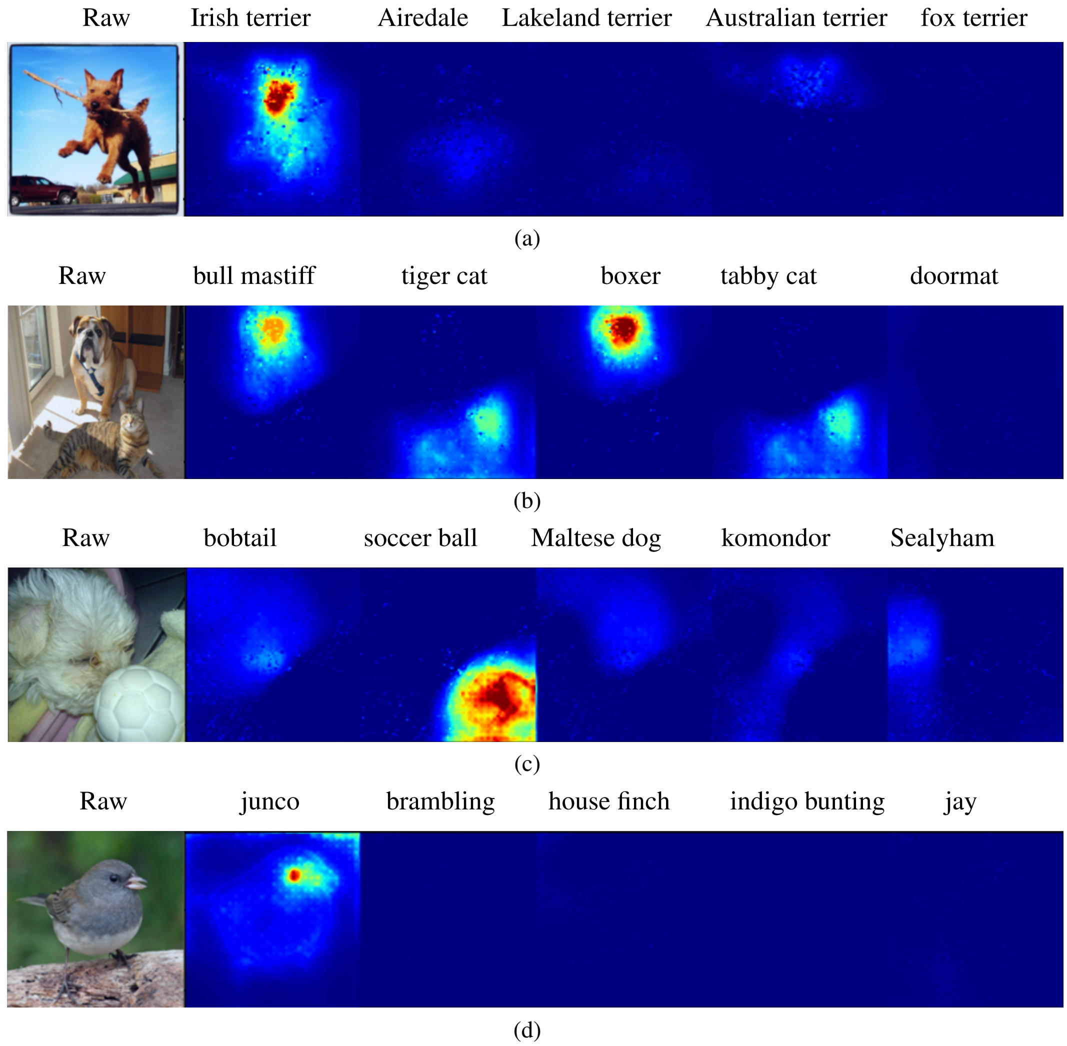

Figure 8: Class Discriminative Visualization for ResNet50. From left to right, they represent top1-top5 classes.

B Sanity Checks

In this section, we present more detailed results for sanity check. We show the reconstruction ability of different layers, and demonstrate the influence of cascade randomization of models on different layers. The results can be seen in Figure 9 for VGG16, and Figure 10 for ResNet50. It can be seen that the low layers of model can emerge corresponding features, and then highlight some of them according to the high-layer attention. In this way, if high layers of a model have been randomized, the reconstruction of low layer can still recognize and discard some irrelevant input features, until they have been randomized too, and then become meaningless. It is noticed that VGG has three FC layers with ReLU activations at the top, according to the answer to predictability questions (1), the noise level depends on the kernel size p, as the FC-layer can be seen as large kernel convolution, such p is too large, so the results in 9 also composite with noise at the top attribution results. These results show that our method can effectively reflect the changes of model parameters.

Additionally, let us concentrate on the columns of 'raw' in Figure 9 and 10, it is clear that the results of bottom layers have more noise than top layers, which have been forecasted in Section4.2.

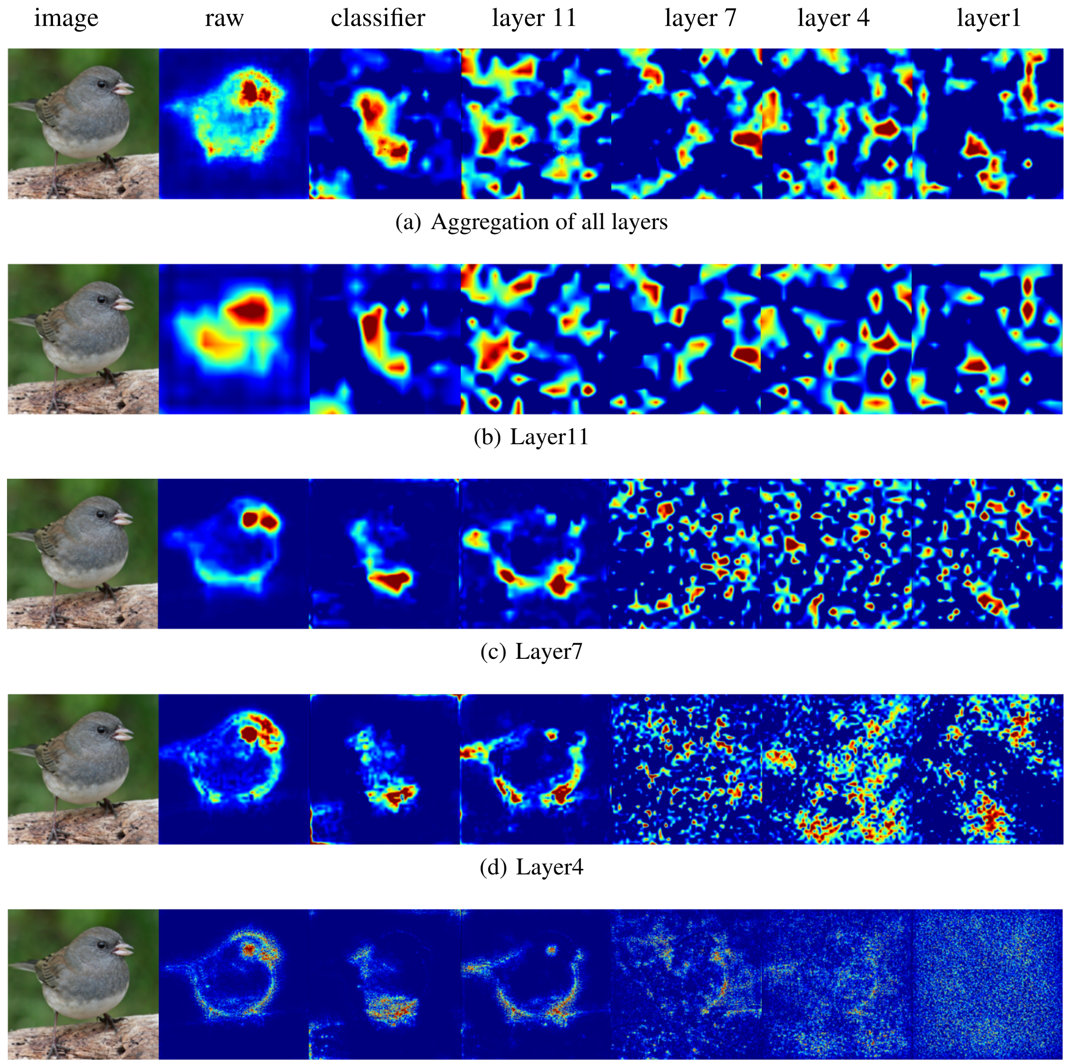

(a) Aggregation of all layers

(b) Layer11

(c) Layer7

(d) Layer4

(e) Layer1

Figure 9: Sanity checks for different layers on VGG16. From left to right, it reflects the cascade randomization of model.

C Experimnental Details of Energy-based Pointing Games

In detail, we use the same setting as Wang et al. (2020): (1) Removing images where an object occupies more than 50% of the whole image to guarantee the bounding box makes sense; (2) Only considered the images with one bounding box which represents the target. We experiment on 500 random selected images from the ILSVRC2012 validation set, each term repeats 5 times and obtains the mean and standard deviation.

D Experimnental Details of Pixel Perturbations

Specifically, our procedure is as follows: for a given value of k, we replace the k pixels corresponding to k most/least salient values with zero pixels. Especially, for GBP and GIG, we add an absolute function to obtain the least differences for LeRF as the least score is not zero but negative values, which means it can also influence the output.

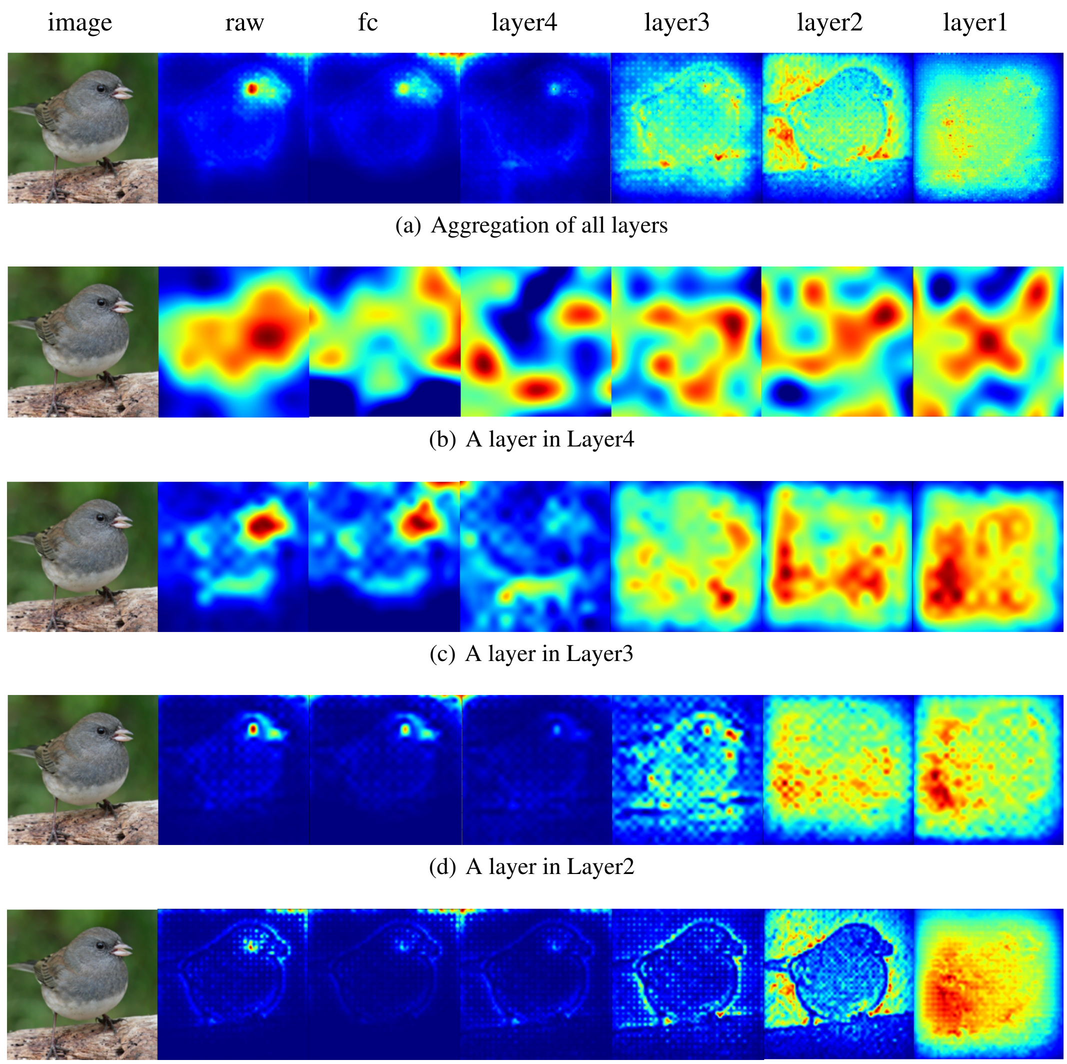

(a) Aggregation of all layers

(b) A layer in Layer4

(c) A layer in Layer3

(d) A layer in Layer2

(e) A layer in Layer1

Figure 10: Sanity checks for different layers on ResNet50. From left to right, it reflect the cascade randomization of model.